Polarized Fluorescence Microscopy of Individual and Many Kinesin Motors Bound to Axonemal Microtubules

Erwin J. G. Peterman,* Hernando Sosa,† Lawrence S. B. Goldstein,† and W. E. Moerner*
*Department of Chemistry, Stanford University, Stanford 94305-5080 and †Department of Pharmacology, Department of Cellular and Molecular Medicine, Howard Hughes Medical Institute, University of California San Diego, La Jolla, California 92093-0683 USA.

ABSTRACT Kinesin is a molecular motor that interacts with microtubules and uses the energy of ATP hydrolysis to produce force and movement in cells. To investigate the conformational changes associated with this mechanochemical energy conversion, we developed a fluorescence polarization microscope that allows us to obtain information on the orientation of single as well as many fluorophores. We attached either monofunctional or bifunctional fluorescent probes to the kinesin motor domain. Both types of labeled kinesins show anisotropic fluorescence signals when bound to axonemal microtubules, but the bifunctional probe is less mobile resulting in higher anisotropy. From the polarization experiments with the bifunctional probe, we determined the orientation of kinesin bound to microtubules in the presence of AMP-PNP and found close agreement with previous models derived from cryo-electron microscopy. We also compared the polarization anisotropy of monomeric and dimeric kinesin constructs bound to microtubules in the presence of AMP-PNP. Our results support models of mechanochemistry that require a state in which both motor domains of a kinesin dimer bind simultaneously with similar orientation with respect to the microtubule.

INTRODUCTION

The kinesin superfamily consists of more than 100 different motor proteins that can move along microtubule tracks and power intracellular motile processes such as organelle transport and cell division (Goldstein and Philp, 1999). The defining characteristic of kinesin is a highly conserved catalytic domain that possesses ATP hydrolytic and microtubule binding activities. Most of the information about the molecular mechanism of action of these motors comes from studies of the founding member of this superfamily called conventional kinesin or kinesin-I (hereafter called kinesin). Kinesin is a tetramer of two pairs of polypeptides, kinesin heavy chain (KHC) and kinesin light chain (KLC). KHC contains the catalytic motor domain and a dimerization domain where the two heavy chains join by α-helical coiled-coil interactions. Thus, each kinesin molecule has two motor domains that appear to coordinate their catalytic activities to generate processive motion (Vale and Milligan, 2000). In spite of considerable advances, the detailed mechanism of this motion is still not fully understood.

Recently, a combination of biophysical approaches has given the first glimpses of the conformational changes likely to be associated with kinesin translocation (Rice et al., 1999). To gain further insight into the structural intermediates of the mechanochemical cycle of kinesin, we have used here polarization spectroscopy of many and single molecules. Polarized optical spectroscopies, like linear dichroism and polarized fluorescence, are well-established techniques in biophysics (Cantor and Schimmel, 1980). The relatively simple addition of polarizers in conventional absorption and fluorescence experiments allows determination of (ensemble-averaged) orientation and orientational dynamics of chromophores (van Amerongen and Struve, 1995). Recently, polarization spectroscopy techniques have been applied to single fluorophores to analyze DNA conformations (Ha et al., 1999), to study the rotation of F1-ATPase (Adachi et al., 2000), and to investigate the acto-myosin system (Sase et al., 1997; Warshaw et al., 1998). The removal of ensemble averaging in these single-molecule experiments can lead to resolution of inhomogeneity due to different static or dynamic states (Moerner and Orrit, 1999; Weiss, 1999; Lu et al., 1998). An additional advantage of working with single molecules is that stochastic processes (such as, for example, motor action) can be followed without the need for synchronization of many molecules. Ultimately, single-molecule fluorescence polarization microscopy could be applied to study conformational changes of moving kinesin molecules.

In this study, we analyze the fluorescence-detected linear dichroism signals of probes attached at specific residues on the kinesin motor domain. We compare the use of a probe attached by a single (monofunctional) or a double (bifunctional) covalent bond. Similar bifunctional probes were recently developed and used to study the acto-myosin system (Corrie et al., 1999). A key advantage of attaching a bifunctional probe to a protein of known atomic structure is that the (average) orientation of the probe with respect to the protein is predetermined (Corrie et al., 1999).

Previously, we reported the use of our fluorescence microscopy method to study the orientation and dynamics of

Received for publication 24 April 2001 and in final form 25 July 2001.

Drs. Peterman and Sosa contributed equally.

Dr. Sosa's present address and to whom requests for reprints should be addressed is Department of Physiology and Biophysics, Albert Einstein College of Medicine, Bronx, NY 10461. Tel.: 718-430-3451; Fax: 718-430-8819; E-mail: hsosa@aecom.yu.edu.

Dr. Peterman's present address is Division of Physics and Astronomy, Vrije Universiteit, Amsterdam, The Netherlands.

© 2001 by the Biophysical Society

0006-3495/01/11/2851/13 $2.00

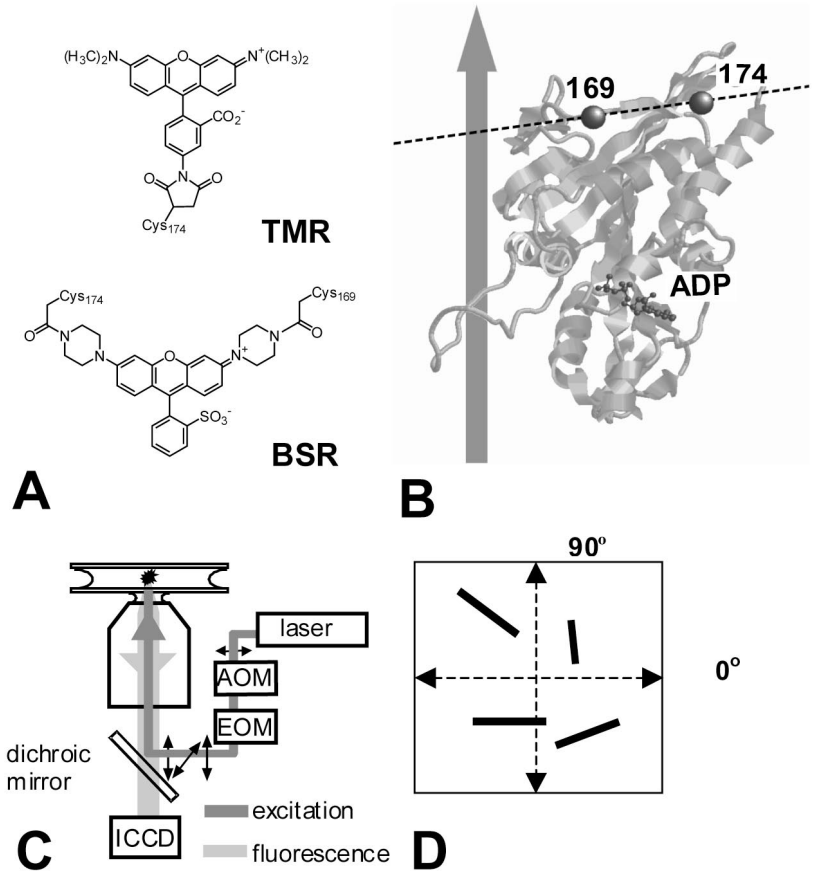

FIGURE 1 Experimental set up. (*A*) Structures of the two fluorescent probes used in this study: tetramethylrhodamine-5-maleimide (TMR) and (bis-((*N*-iodoacetyl)piperazinyl) sulfonerhodamine (BSR). (*B*) Ribbon representation of the kinesin motor domain atomic structure (Kull et al., 1996), showing the two cysteines (cys^{169} and cys^{174}) where the fluorescent probes were attached. The transition dipole moment of BSR is aligned along the long axis of the three coplanar rings of the fluorophore (Penzkofer and Wiedmann, 1980) and is parallel to the line connecting the two thiol groups of the protein to which it is bound. Hence, attaching BSR to the indicated cysteines is expected to orient the fluorescence dipole in the kinesin structure as shown (*dashed line*). The kinesin constructs KMC (monomeric) and KCL (dimeric) have only one cysteine residue at position 174 and were labeled with TMR. The construct KMC2 (monomeric) has two cysteines at positions 169 and 174 and was labeled with BSR. The arrow shows the relative position and orientation of the microtubule according to cryo-electron microscopy docking models (Sosa et al., 1997). (*C*) Schematic view of the fluorescence polarization microscope setup. *AOM*, acousto-optic modulator; *EOM*, electro-optic modulator; *ICCD*, intensified charge-coupled device camera. See text for details. (*D*) Schematic view of the experimental position of axonemes in the coverslip plane (*xy*-plane) with random orientations.

the kinesin motor bound to axonemal microtubules in the presence of different nucleotide analogues (Sosa et al., 2001). Here we focus on a detailed description of the experimental approach and data analysis applied, and compare a monofunctional and a bifunctional fluorescent probe attached to kinesin. Finally, we compare the orientation of monomeric and dimeric kinesin constructs bound to axonemal microtubules in the presence of the nonhydrolyzable ATP analogue, AMP-PNP. The resulting data indicate that, in the presence of AMP-PNP, both motor domains of the dimeric kinesin motor are bound to the microtubule.

MATERIALS AND METHODS

Kinesin constructs

Kinesin proteins were expressed as bacterial recombinant proteins comprising ubiquitous human kinesin heavy-chain (KIF5B) amino acid residues 1–559 or 1–349 with a C-terminal six-histidine tag. To ensure specific labeling with SH-reactive fluorophores, most of the native cysteines were replaced by alanines. Three different constructs were created for this work: KMC, KCL, and KMC2. KMC is composed of KIF5B amino acids 1–349 with all cysteines but cys^{174} replaced by alanines plus the C-terminal tag (HHHHHH). KCL is composed of KIF5B amino acids 1–559 with all cysteines but cys^{174} replaced by alanines plus the C-terminal tag (VEHHHHHH). KMC2 is similar to KMC but Thr^{169} was replaced by a cysteine. KMC and KMC2 do not have the dimerization domain and thus are monomers, whereas KCL is dimeric. Site-directed mutagenesis was performed using the Quick Change protocol (Stratagene, La Jolla, CA). Oligonucleotides were designed to include the desired mutations and a silent mutation with a new restriction site that allowed verification of the new sequence in the plasmids. We started our constructs from a pet23b plasmid containing the coding sequence for KIF5B aminoacids 1–559. We verified the sequence of all the constructs by sequencing. Figure 1 *B* shows the location of the unique reactive cysteines of these kinesin constructs.

The kinesin constructs were expressed in *Escherichia coli* BL21 cells. A single colony containing the desired plasmid was grown overnight in a small volume (5–10 ml) of media (10 g/L Bacto-Tryptone, 5 g/L yeast

extract, 5 g/L NaCl, 2 g/L $MgSO_4$, 1g/L casamino acids, 200 mg/L ampicilin) at 37°C with 2 g/L $MgSO_4$, 240–250 rpm shaking. The overnight culture was used to inoculate a bigger volume (1:100) of media, which was incubated at 37°C with 240–250 rpm shaking for about 5 h up to an OD of 0.8–1.5 cm^{-1}. Protein expression was then induced with 0.5 mM IPTG overnight at room temperature. Cells were then harvested, resuspended (50 mM TRIS pH = 7, 50 mM NaCl, 5 mM $MgCl_2$, 7 mM β-mercaptoethanol, 1 mM PMSF, 0.1 tablet ml^{-1} Complete Mini-EDTA-free protein inhibitor cocktail (Boehringer, Mannheim, Germany)), and disrupted by three passes through a French press. Insoluble material was removed by centrifugation (45 min, 100,000 × *g*, 4°C). The supernatant was incubated with gentle rolling with 1–3 ml of Ni-NTA resin (Qiagen Inc, Valencia, CA) for 45 min at 4°C. The protein bound to the resin was washed twice with 10 volumes of resuspension solution and once with 10 volumes of resuspension solution with added 50 mM imidazole and 50 μM ATP (wash I). The resin was transferred to a column. Ten milliliters of wash-I solution were passed through the column and the protein eluted with resuspension solution made with 500 mM imidazole and 50 μM ATP (elution I). One-half-milliliter aliquots were collected, and the protein peak position was determined by a colorimetric protein assay.

Protein labeling

After the nickel-affinity purification, the protein constructs were passed through a desalting column preincubated with labeling buffer (80 mM PIPES pH = 6.8, 2 mM $MgCl_2$, 1 mM EGTA, 50 μM ATP). The concentration of eluted protein was determined and the reactive dye was added immediately. We labeled the single cysteine constructs KMC and KCL with the monofunctional thiol-reactive dye tetramethylrhodamine-5-maleimide (TMR) and the double cysteine one KMC2 with the thiol bifunctional reactive dye bis-((*N*-iodoacetyl)piperazinyl) sulfonerhodamine (BSR) (both dyes from Molecular Probes, Eugene, OR) (Fig. 1 *A*). The labeling mixture had a ratio of 2:1 of TMR to KMC or KCL and 1:1 BSR to KMC2. The mixture was incubated overnight, and the next day the reaction was stopped by adding 1 mM DTT. The mixture was then passed through a desalting column pre-equilibrated with labeling buffer with 1 mM DTT to eliminate the unreacted dye. The resulting protein solution was made 19% sucrose, aliquoted, flash frozen, and stored at −80°C. We estimated the amount of labeled protein by spectrophotometry to be 100% for KMC-TMR, 30% for KCL-TMR and 60% for KMC2-BSR. We verified by mass spectrometry that the double cysteine construct KMC2 was labeled with one BSR molecule that had reacted with both thiols. Overnight digestion of KMC2-BSR with endoproteinase Lys-C followed by liquid chromatography mass spectroscopy (LC-MS) showed a product with mass corresponding to a peptide with the two cysteines linked to the BSR probe (predicted mass, 2884.148 daltons; found mass, 2884.15 daltons). Digestion with trypsin (for which there is a cleavage site at residue R between the cysteines) resulted in a product with mass corresponding to the two cysteine-containing peptides hydrolyzed at the middle R residue (expected mass increment of 18 daltons for hydrolysis) but still joined by the probe cross-link (predicted mass, 2902.15 daltons; found mass, 2902.45 daltons). These protease digestion/LC-MS experiments confirmed that each of the two functional groups of BSR was linked to a cysteine on KMC2. The distance, 16 Å between the Cα atoms, as measured from the crystal structure (Kull et al., 1996), and orientation between the two reactive SH groups at cys^{169} and cys^{174} seems optimal to cross-link them with BSR. Moving one cysteine to an adjacent position one amino acid further away in the sequence (cys^{168}–cys^{174}) resulted in very low yields of protein with BSR attached by its two functional groups. The three cysteine-substituted and labeled constructs used in this work showed microtubule-stimulated ATPase activity (V_{max} 29–55 ATP s^{-1} $head^{-1}$, in 12 mM PIPES, pH 6.8, 0.5 mM ATP, 2 mM $MgCl_2$, 1 mM EGTA) in a coupled enzymatic assay (Enz-Check phosphate assay kit, Molecular Probes). The dimeric construct KCL-TMR showed processive motion in a single-molecule motility assay. Protein concentration was determined colorimetrically against BSA standards. The concentration of the longer dimeric construct, KCL-BSR, was determined from Coomasie stained SDS-PAGE gels using BSA standards. We also created a dimeric construct with a bifunctional probe, KCL2-BSR, but the yield of functional protein was very low. Consequently, our comparison between monomeric and dimeric kinesin is based on the monofunctionally labeled constructs KMC-TMR and KCL-TMR.

Axonemes

We used axoneme preparations in our experiments as a source of microtubules because they give longer and straighter filaments than in vitro polymerized microtubules. In addition, all protofilaments in the axonemal microtubules are parallel to the axoneme axis, so that variability due to protofilament twist angle is eliminated. We also performed experiments with in vitro polymerized microtubules and the results were consistent with the ones presented here but more variable (data not shown). We attribute this variability to the fact that in vitro microtubules are more easily distorted and to the presence of other assembly forms such as open sheets and microtubules with different number of protofilaments and supertwist angles.

Axonemes were prepared from sea urchin sperm by double salt extraction (Gibbons and Fronk, 1979). Packed sea urchin sperm (gift from V. Vaquier Lab, University of California—San Diego) were homogenized in 20% sucrose and centrifuged (2988 × *g*) for 5 min in a Sorvall SS34 rotor. The supernatant was collected and centrifuged (30,597 × *g*) for 15 min at 4°C. The resulting pellet was resuspended in resuspension buffer (30 mM HEPES pH = 7.4, 600 mM KCl, 5 mM $MgSO_4$, 1 mM DTT, 0.5 mM EDTA, 1% IGEPAL CA-630 detergent (Sigma)), homogenized, and centrifuged again (30,587 × *g*, 20 min, 4°C). The resulting pellet was resuspended in resuspension buffer without detergent and centrifuged as before. The pellet was then finally resuspended (30 mM HEPES pH = 7.4, 100 mM KCl, 5 mM $MgSO_4$, 1 mM DTT, 0.5 mM EDTA, 50% glycerol) and stored at −20°C. The concentration of tubulin in the axoneme preparations was estimated by running an aliquot on an SDS gel and calculating by densitometry the amount of protein in the band corresponding to tubulin. For calibration, different amounts of BSA standards were run on adjacent lanes.

Sample preparation for the polarization measurements

Fluorescence polarization was measured on axonemes with bound kinesin molecules. The experimental mix contained axonemes and labeled kinesin in the assay buffer (12 mM PIPES pH = 6.8, 2 mM AMP-PNP, 2 mM $MgCl_2$, 1 mM EGTA, 10 mM glucose, 0.1% β-mercaptoethanol, 0.1 mg/ml catalase, 0.03 mg/ml glucose oxidase, 7.5 mg/ml BSA). Four microliters of this mix were placed between two clean glass coverslips (Number 1, 0.13–0.17-mm thick). Kinesin concentration was ~75 nM in the multimolecules experiments and ~0.75 nM in the single-molecule ones. The calculated axonemal tubulin $\alpha\beta$ dimer concentration in the experimental mix was 300–600 nM, so that there was always an excess of tubulin binding sites for kinesin to bind.

Fluorescence polarization microscopy

The fluorescence of kinesin bound to axonemes was imaged using the setup shown in Fig. 1 *C*. Excitation light (532 nm, ~1 kW/cm^2 at the sample) was provided by a diode-pumped, frequency-doubled Nd:YAG laser (Millenia, Spectra Physics, Mountain View, CA). The polarization of the laser light in the sample plane was alternated between 0°/90°, 0°/45°/90°/135°, or 0°/30°/90°/120° linear polarizations using an electro-optic modulator (M350–50, Conoptics, Danbury, CT). An acousto-optic modulator (1205-603D, Isomet, Springfield, VA) was used to adjust the inten-

sities of the differently polarized excitation light, to avoid selective bleaching of the fluorophores in the experiments with many kinesin molecules bound to axonemes. In the single-fluorophore experiments, the images were corrected during analysis for differing excitation intensities. The excitation light entered the epi-fluorescence port of an inverted optical microscope (Diaphot 200, Nikon Inc., Melville, NY) and was reflected (after defocusing with respect to the emitted light by a lens) toward the objective lens (Nikon 100×, 1.4 NA, PlanApo, oil immersion) with a dichroic mirror (DR540LP or DR545LP, Chroma, Brattleboro, VT). After reflecting from the dichroic mirror, the intensity polarization ratios were 45:1, 18:1, 390:1, and 33:1 for the 0°, 45°, 90°, and 135° cases, respectively. When four polarization axes were used, a λ/4 plate (Tower Optical, Delray Beach, FL) was placed after the EOM and two identical dichroic mirrors with planes of reflection perpendicular to each other were used to partially compensate phase distortions introduced by a single dichroic (Dr. R. Hochstrasser, personal communication). The emitted light was imaged via the dichroic mirror, a bandpass filter (570DF40, Chroma), a 532-nm notch filter (supernotch 532, Kaiser, Ann Harbor, MI), and a 4× relay lens on an intensified, frame-transfer CCD camera (Ipentamax, Princeton Instruments, Trenton, NJ). The total optical magnification of the microscope and camera was 275×. Three phase-locked function generators controlled and synchronized the CCD camera, the electro-optic modulator, and the acousto-optic modulator, such that images were recorded at 10 Hz upon excitation with alternating polarization. Data and image analysis were performed using custom-written software.

The fluorescence along axoneme segments or single fluorescent spots was measured by integrating regions of interest in the images. The intensity corresponding to each excitation polarization was averaged over several image frames after subtracting the background fluorescence (intensity on an area devoid of axonemes and adjacent to the region of interest) and applying a correction factor to account for differences in the excitation intensity and transmission through the optics. From these averaged intensities, the reduced linear dichroism (LD) was calculated (van Amerongen and Struve, 1995),

$$\mathrm{LD}_{0-90} = \frac{I_{90} - I_0}{I_{90} + I_0} \tag{1}$$

in which $I_{0/90}$ is the fluorescence intensity upon excitation with polarization along the x (0°) or y axis (90°). We define the xy-plane as the plane of the microscope stage. Axonemes lie on the coverslips in this plane (Fig. 1 *D*). It should be noted that, in a previous publication (Sosa et al., 2001), we used the term polarization ratio PR instead of LD. We estimated that, in our experimental conditions, the error in estimating LD_{0-90} for axonemes decorated with many labeled kinesins is ± 0.02 LD_{0-90} units. This is the standard deviation of a set of LD_{0-90} values taken along the same axoneme or from several axonemes with an orientation close to 45° (where the expected LD_{0-90} values are close to zero). The time scale of our LD measurements is 100 ms (time to collect each image). Thus, the order or disorder values reported below are on this time scale and not on the time scale of the fluorescence lifetime (ns) as in typical measurements of fluorescence anisotropy or polarization (Cantor and Schimmel, 1980).

RESULTS AND ANALYSIS

Axonemes decorated with many kinesin motors

To obtain information on the orientation of kinesin motor domains bound to microtubules, we studied kinesin-decorated axonemes with fluorescence-detected linear dichroism microscopy. Figure 2 shows an image pair with three axonemes decorated with many kinesin-labeled molecules in the presence of AMP-PNP. The two images correspond to two different directions of the linearly polarized excitation light (*arrows*). In the left image, the horizontally oriented axoneme gives strong fluorescence compared to that for the nearly vertically oriented axonemes, and vice versa for the right image. In this example, the kinesin construct used is the monomeric one labeled with a bifunctional rhodamine derivative (KMC2-BSR). Among the different constructs that we used, KMC2-BSR gave the strongest fluorescent anisotropy (in the presence of AMP-PNP), which is clearly shown in this image pair. More light is emitted when the exciting light is perpendicular to the axoneme axis.

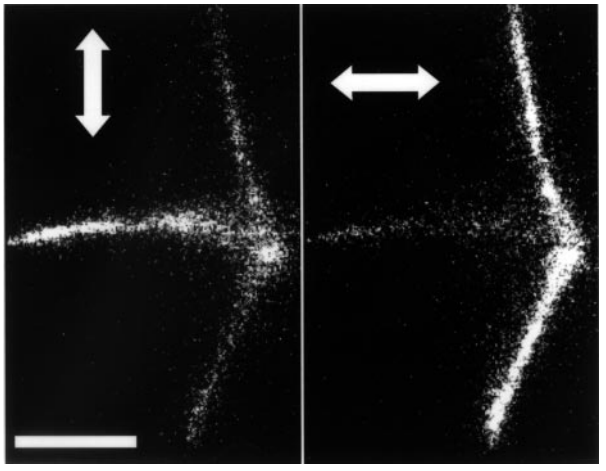

FIGURE 2 Fluorescence image of axonemes decorated with many molecules. In this example, the axonemes are decorated with KMC2-BSR molecules in the presence of AMP-PNP. The arrows indicate the polarization axis of the exciting light. White scale bar in bottom left panel: 3 μm.

Theory

To quantify the observed anisotropy, we measured the intensity of the emitted fluorescence on an axoneme segment with hundreds of individual labeled kinesin molecules. We used excitation light with either of two perpendicular polarizations and calculated the ratio LD_{0-90} (Eq. 1). Because of the cylindrical symmetry of kinesin binding sites on the axonemes, LD_{0-90} is sensitive to the axial angle of the fluorophore relative to the axoneme long axis (β) and the angle (ω) the axoneme makes in the plane of the coverslip with the x axis. In the appendix, we derive that, theoretically, LD_{0-90} can be expressed as

$$\mathrm{LD}_{0-90}(\beta, \omega) = \frac{-3\cos(2\omega)}{1 + 4/(3\cos^2(\beta) - 1)} \tag{2}$$

This equation ignores effects of mobility of the fluorescent probes, which, even for bifunctional probes, can be considerable (Corrie et al., 1999). A more realistic expression can be derived by modeling this mobility as a fast motion of the transition dipole moment within a cone (wobble) with half angle Γ (Lipari and Szabo, 1980). In the appendix, it is shown that LD_{0-90} can be expressed as a function of the

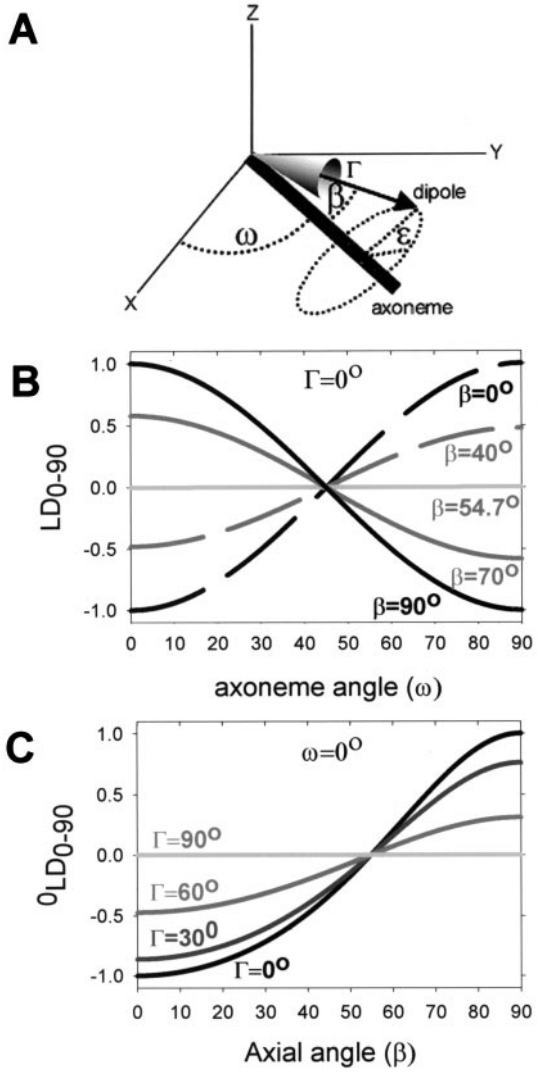

FIGURE 3 Linear dichroism, LD_{0-90}, for an array of many fluorophores with cylindrical symmetry. (*A*) Definition of the geometry and angles used to calculate LD_{0-90} for microtubules decorated with many kinesin molecules. ω is the angle of the axoneme in the *xy*-plane. β is the mean axial angle of the fluorophore with the axoneme axis. ϵ is the angle of the fluorophore around the axoneme long axis. Γ is the half angle of a cone in which the fluorophore is able to pivot. (*B*) Theoretical curves of LD_{0-90} versus the angle ω (deg) for several β values when the probe is nonmobile ($\Gamma = 0°$). (*C*) Effect of increasing mobility (Γ angle) on the maximum polarization ratio ${}^0LD_{0-90}$ as a function of the axial angle β (deg).

angle of the axoneme in the plane of the coverslip (ω), the mean axial angle between the transition dipole moment of the probe and the axoneme (β), and the mobility cone half angle (Γ) (see Fig. 3 *A* for a graphical definition of the angles) as

$$LD_{0-90}(\Gamma, \beta, \omega) = \frac{-3\cos(2\omega)}{1 + 8/[3\cos^2(\beta) - 1]\cdot[\cos(\Gamma) + \cos^2(\Gamma)]} \quad (3)$$

In the absence of mobility ($\Gamma = 0°$) Eq. 3 simplifies to Eq. 2. Figure 3, *B* and *C*, shows the influence of the angles ω, β, and Γ on the LD values calculated using Eqs. 2 and 3. In Fig. 3 *B*, the effect of the fluorophore axial angle β on LD_{0-90} as a function of the axoneme angle ω is shown for the case of no probe mobility ($\Gamma = 0^o$). The curves are symmetric about the *x* axis and reach maximum values when the axoneme is parallel to either polarization axis ($\omega = 0$ or $\omega = 90°$). We will call these two LD values ${}^0LD_{0-90}$ and ${}^{90}LD_{0-90}$, respectively (${}^0LD_{0-90} = -{}^{90}LD_{0-90}$). ${}^0LD_{0-90}$ reaches the maximum value of 1 when the fluorophores are perpendicular to the axoneme ($\beta = 90°$). All LD_{0-90} values are zero when $\beta = 54.7°$ (magic angle). When the fluorophores are parallel to the axoneme axis ($\beta = 0°$) ${}^0LD_{0-90}$ is equal to -1. Mobility of the probe has the effect of reducing proportionally all LD_{0-90} values. This is shown in Fig. 3 *C*, where the maximum ${}^0LD_{0-90}$ as a function of the axial angle β is plotted for several different values of the cone half angle Γ.

Experimental results

In Fig. 4, the experimentally determined LD_{0-90} values are plotted as a function of the axoneme angle ω for axonemes decorated with KMC-TMR (*A*), KCL-TMR (*B*), and KMC2-BSR (*C*). Both kinesin constructs, labeled with the monofunctional probe (KMC-TMR and KCL-TMR), gave much lower LD_{0-90} values than the construct with the bifunctional probe (KMC2-BSR). ${}^0LD_{0-90}$ is up to 10 times higher for KMC2-BSR (note the different vertical scales). The low polarization observed for the monofunctional probe could indicate that the probe axial angles are close to 54.7°, that the axial angles from motor to motor are more random, or that the probes or motors are highly mobile. Because this probe is only attached with a single bond to the protein (compared to two bonds for BSR), it is likely to have more freedom to pivot around its single attachment point and hence to be more mobile than the bifunctional one. Our single-molecule analysis (next section) confirms that the monofunctional fluorophore is more mobile than the bifunctional one.

There is scatter in the observed LD_{0-90} values at each axoneme angle, ω. A fraction of this variability is associated with the noise in the determination of LD_{0-90}. We estimated that, in our experimental conditions, this noise is ± 0.02 LD_{0-90} units (see Methods). This variability is an important fraction of the scatter present in the data associated with the constructs labeled with the monofunctional probe (KMC-TMR, KCL-TMR) (Fig. 4, *A* and *B*) due to their lower overall LD_{0-90} values. For KMC2-BSR (Fig. 4 *C*), the observed scatter is higher than the measurement noise and increases as ω approaches 0^o or 90^o. In this case, fluorophore disorder induced by surface adsorption or microtubule flattening could affect the axonemes randomly to produce this variability. Because these physical effects tend only to reduce the polarization anisotropy from the ideal

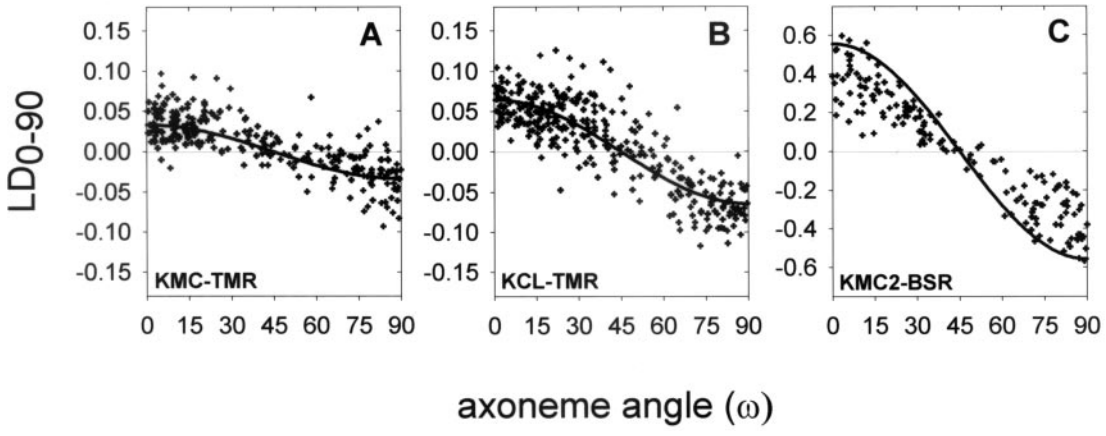

FIGURE 4 Experimentally determined LD_{0-90} as a function of the axoneme angle ω (deg). (*A*) Axonemes decorated with KMC-TMR. (*B*) Axonemes decorated with KCL-TMR. (*C*) Axonemes decorated with KMC2-BSR. Note the different vertical scale in *panel C*. All experiments were done in the presence of AMP-PNP. The superimposed curves are fits to Eq. 3 ($\beta = 56^o$, 58^o, 75^o and $\Gamma = 50^o$, 50^o, 32^o, respectively, for *panels A*, *B*, and *C*). In *A* and *B*, all points were included in the fitting, whereas in *C*, only the maximum LD_{0-90} observed at each 10^o interval.

value if cylindrical symmetry were preserved, the LD_{0-90} values scatter from 0 to the maximum possible values (line in Fig. 4 *C*).

Single kinesin motors bound to axonemes

Theory

From the combined signal of many molecules, it is not possible to separate unambiguously the contributions of the probe axial angle and the probe mobility to the resulting LD_{0-90} values. To estimate the amount of probe mobility, we determined the linear dichroism of single molecules. In these experiments, we measured the emission intensity upon excitation with four alternating excitation polarizations, forming two perpendicular pairs (0°/45°/90°/135° or 0°/30°/90°/120°). From these intensities, two distinct linear dichroism values were calculated, LD_{0-90} and LD_{45-135} (or LD_{30-120}).

By comparing two linear dichroism values for many individual molecules, it is possible to obtain information on the mobility of the fluorophore. For any single dipole, defined in three dimensions by polar angles ϕ and θ, the LD_{0-90} has a defined relationship with the $LD_{\eta\text{-}\eta+90}$ calculated using another perpendicular pair of polarization axes at an angle η. This relationship is strongly dependent on the mobility of the probe. In the, Appendix we derive the following expression (Eq. 4) that relates $LD_{\eta\text{-}\eta+90}$ with the average azimuthal angle of the dipole in the *xy* plane (ϕ), the angle of the dipole with respect to the *z* axis (θ) and a semiangle Γ in which the probe is able to pivot very rapidly from its attachment point:

$$LD_{\eta-\eta+90^\circ}(\phi, \theta, \Gamma) = \frac{3\sin^2(\theta)[2\cos^2(\phi-\eta)-1]}{3\cos^2(\theta)-1-4/[\cos(\Gamma)+\cos^2(\Gamma)]} \quad (4)$$

Using Eq. 4, we calculated the values of LD_{0-90} and LD_{45-135} for 2000 randomly oriented dipoles (we verified that the randomly selected ϕ and θ were uniformly distributed among all possible values) assuming different values of the cone angle Γ. Plots of LD_{45-135} versus LD_{0-90}, as obtained from these random simulations, are shown in the top three left panels of Fig. 5. For immobile dipoles ($\Gamma = 0$), all points (each representing a single randomly oriented dipole) fall on a circle. For more mobile dipoles, both LD values are reduced, resulting in positions closer to the origin of the plot. When $\Gamma = 90°$, all points fall on the origin (both LD values are equal to zero). We define *r* for each point as $LD_{0-90}^2 + LD_{45-135}^2 = r^2$, which is the distance from the origin (0, 0). Thus, for immobile dipoles, $r = 1$, and increases in mobility ($\Gamma > 0$) results in $r < 1$ up to the extreme when $\Gamma = 90^o$ that the value of *r* is zero for any fluorophore orientation. The top three right panels of Fig. 5 show the *r* value distributions for the simulated data. The mean and peak *r* value of the distribution moves toward lower values as the mobility angle Γ increases. Figure 6 shows the mean value of the *r* distributions as a function of the mobility cone semiangle Γ (*dotted line*). The solid line takes into account the fact that, depending on their orientation, some fluorophores absorb less light and are not detectable. In particular, the less mobile fluorophores, which are nearly parallel to the *z* axis, have low probability of being excited and detected with light polarized in the *xy*-plane. The solid line in Fig. 6 excludes dipoles that have a projection in the *xy*-plane of less than 20% of their total magnitude.

The above discussion assumes that the measurements are done with a pair of orthogonal axes separated by 45^o, LD_{0-90} and LD_{45-135}. Similar information can also be obtained with axes separated by different angles. In some of our experiments, we excited with 0^o, 30^o, 90^o, and 120^o polarization directions and calculated LD_{0-90} and LD_{30-120}.

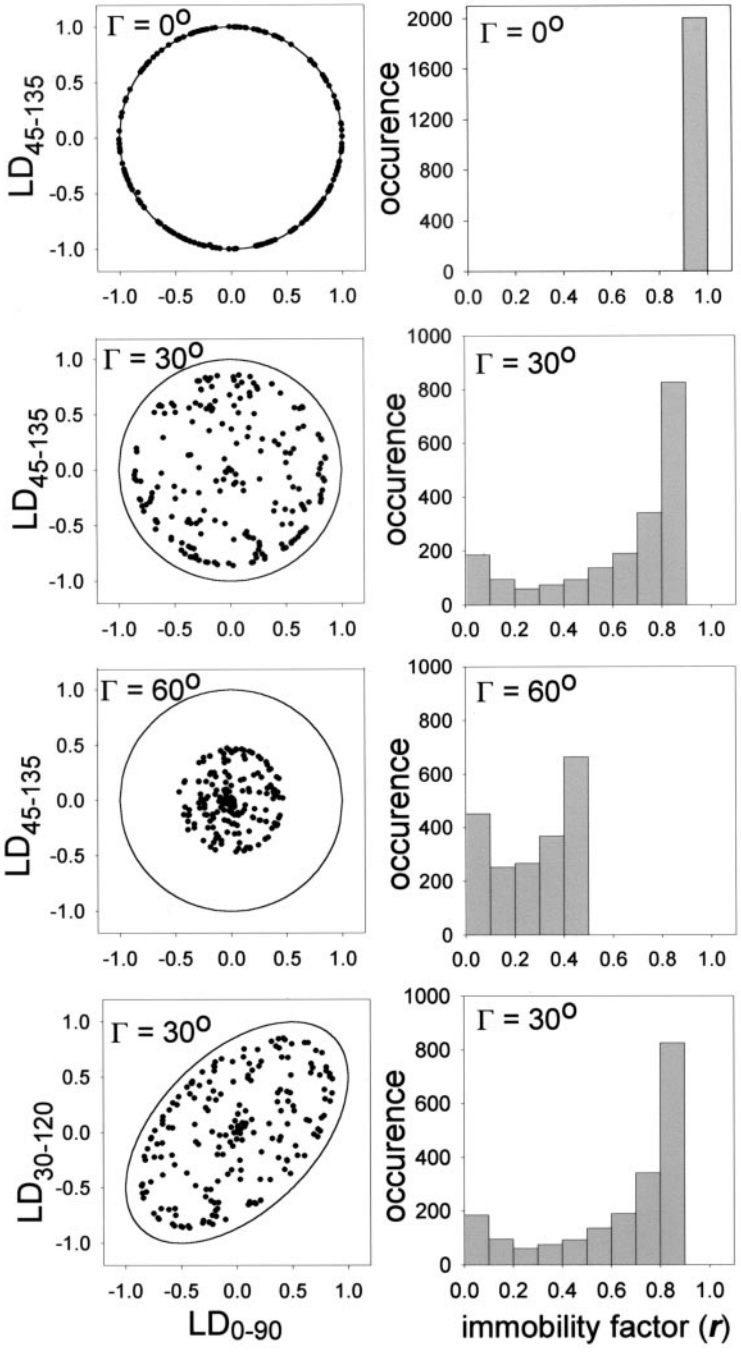

FIGURE 5 Simulations of the LD values of randomly oriented single molecules, assuming disorder defined by the cone half angle (Γ) of 0°, 30°, and 60°. *Left:* Scatter plots LD_{45-135} versus LD_{0-90} and LD_{30-120} versus LD_{0-90} (*bottom*). Each point on the scatter plots corresponds to a single molecule with a particular orientation. Two hundred random orientations were included in these plots. *Right:* immobility factor (*r*) histograms. For the histograms 2000 dipole random orientations were simulated.

In this case, an LD_{30-120} versus LD_{0-90} scatter plot for probes with no mobility will form an ellipse instead of a circle (Fig. 5, *bottom*). This ellipse is defined by

$$LD_{30-120} = \tfrac{1}{2} \cdot LD_{0-90} \pm \sqrt{\tfrac{3}{4} - \tfrac{3}{4} \cdot LD_{0-90}{}^2} \qquad (5)$$

In this case, we use a similar definition for the immobility factor (*r*), namely the distance between the origin and the data point (R_d) divided by the radial distance (R_e) between the origin and the ellipse crossing the data point (this distance is always 1 for LD_{0-90} versus LD_{45-135}). R_e is

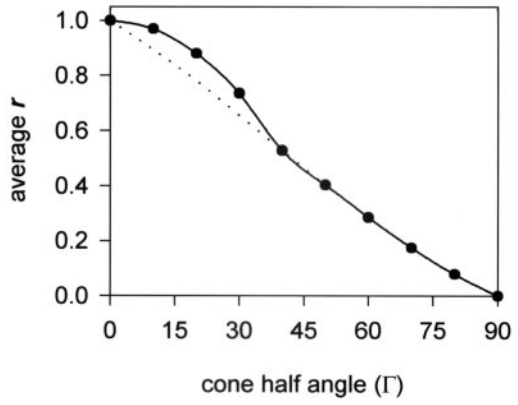

FIGURE 6 Average mobility factor r (obtained from simulations as shown in Fig. 5) as a function of the cone half angle Γ. For the solid line, only fluorophores with an x–y projection length of at least 20% of the total length (which we estimate is our detection limit) were taken into account. For the dotted line, all fluorophores were taken into account.

calculated from the position of the data point in the scatter plot by

$$R_e(\alpha) = \frac{1}{\sqrt{\frac{4}{3}[\sin(\alpha) - \frac{1}{2}\cdot\cos(\alpha)]^2 + \cos^2(\alpha)}} \quad (6)$$

where α is the angle of the data point with the horizontal axes in an LD_{30-120} versus LD_{0-90} plot. The immobility factor is then calculated as

$$r = R_d/R_e$$

As before, $r = 1$ for an immobile dipole and $r = 0$ for a fully mobile one. A plot of the average r value versus Γ for LD_{0-90} and LD_{30-120} gave the same relationship as the one shown in Fig. 6 for LD_{0-90} and LD_{45-135}.

Experimental results

To estimate the amount of fluorophore mobility on our labeled proteins, we measured their single-molecule LD for two sets of axes and calculated the r values. Figure 7 shows an image of an axoneme sparsely covered with labeled kinesin molecules. Time courses of the fluorescence intensity of one of these spots (Fig. 7, *right*) reveal approximately constant values until a discrete photobleaching event at ~5 s, typical for single-molecule recordings (Funatsu et al., 1995). The fluctuations of each of the signals about their mean values are due to photon counting statistics and electronic noise of the detector. From traces like these, we calculated LD_{0-90} and LD_{45-135} (or LD_{30-120}), and from these values, the immobility factor (r). Scatter plots and histograms of r are shown in Fig. 8 for the three constructs studied in this work, all in the presence of AMP-PNP. The average value of r for the constructs labeled with the monofunctional probe (KMC-TMR, KCL-TMR) is 0.4, whereas the average r is 0.7 for the construct labeled with the bifunctional probe (KMC2-BSR). The higher r in the case of KMC2-BSR indicates that the double attachment of the fluorophore is much more rigid than the single attachment. With the average r values and using Fig. 6, we estimate a mobility cone semiangle Γ of 50 ± 5° for both constructs labeled with TMR and 32 ± 5° for KMC2-BSR.

Having determined estimates of the mobility cone angle, we estimated the axial angle β between the probe and the axoneme using Eq. 3 and the curves of LD_{0-90} versus ω (Fig. 4) for axonemes covered with many kinesin motors. The estimated axial angles were, respectively, 56°, 58°, and 75° for KMC-TMR, KCL-TMR, and KMC2-BSR.

Thus, both the dimeric and monomeric kinesin constructs labeled with TMR gave very similar mobility and orientation values (±2°). This indicates a similar microtubule-bound configuration (in the presence of AMP-PNP) for the two heads of a kinesin dimer or the single head of a kinesin

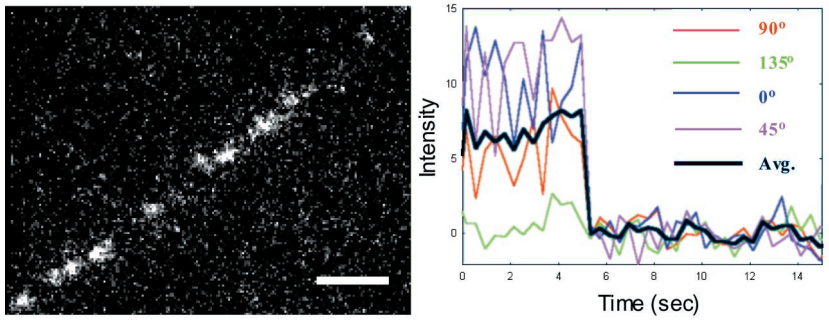

FIGURE 7 Single molecules on axonemes. The left panel shows an image with several fluorescent spots along an axoneme. In this example, the axoneme is sparsely decorated with KMC2-BSR molecules in the presence of AMP-PNP. Scale bar: 3 μm. The right panel shows the time traces of the fluorescent intensity from one of the fluorescent spots on the left panel image. The different color traces correspond to the four different excitation polarization axes used (0°, 90°, 45°, 135°). The black trace corresponds to the average signal obtained with the four excitations. Typical of single-molecule recording, the average intensity remains approximately constant until the fluorophore bleaches producing a single step drop in intensity.

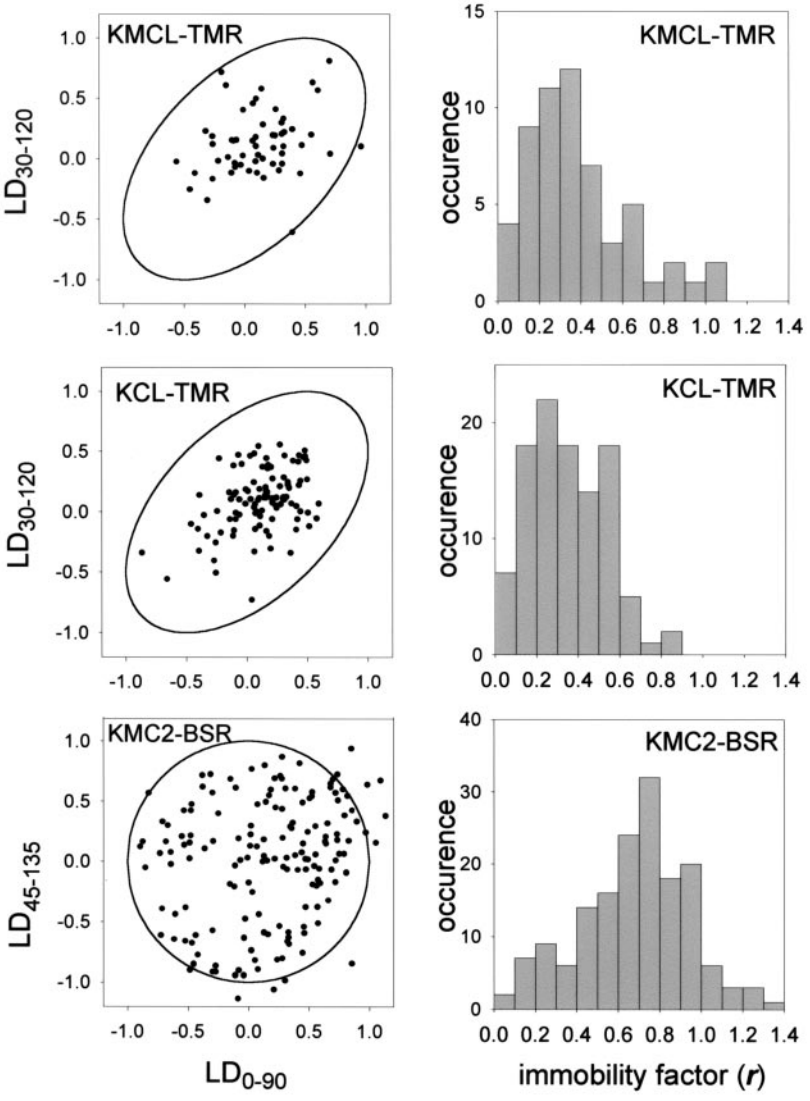

FIGURE 8 Scatter plots (*left*) and histograms of mobility factors *r* (*right*) measured for single kinesin molecules on axonemes in the presence of AMP-PNP. From top to bottom: KMC-TMR, KCL-TMR, KMC2-BSR.

monomer. Because we have not measured the orientation of each of the two motor domains within the kinesin dimer, it is conceivable that they have different configurations and that their added signal resembles the one produced by the monomeric construct. However, cryo-electron microscopy reconstructions have indicated that the kinesin motor domain interacting with the microtubule has a similar configuration in monomeric and dimeric constructs (Sosa et al., 1997; Hoenger et al., 1998). Thus, if the orientation of an individual motor domain within the dimer is similar to the orientation of the motor domain within the monomer, then a similar angle and mobility for both constructs indicates that both motor domains within the dimer have a similar configuration.

The difference in the average axial angle between the TMR- and BSR-labeled constructs is likely due to the difference in the geometry of attachment of the two probes (Fig. 1 *A*). In the case of KMC2-BSR, the average axial orientation (75°) determined in this work is consistent with the motor domain orientation previously estimated by cryo-electron microscopy (Fig. 1 *B*).

DISCUSSION

To study the orientation and dynamics of kinesin motors bound to microtubules, we have used single- and multiple-fluorophore polarization spectroscopy. Several techniques were implemented to extend the information from what is possible to obtain by bulk polarization measurements: 1) the use of a microscope to select the signal from molecules interacting with microtubules, 2) the use of more than two

excitation polarization axes to resolve ambiguities derived from the combined effects of mobility and orientation on fluorescence anisotropy, and 3) the use of a bifunctional probe to relate the orientation of the fluorophore with the orientation of the kinesin motor domain.

Comparison between monofunctional and bifunctional probes

In this work, kinesin was labeled with two distinct probes: a monofunctional one (TMR) and a bifunctional one (BSR). We found that the mobility of the monofunctional one is higher than that of the bifunctional one. This is not necessarily surprising given the double attachment of the probe to the protein. However, in a previous pioneering fluorescence polarization study, no difference was observed between a bifunctional and a monofunctional probe attached to myosin light chains (Corrie et al., 1999). In this study, a mobility cone semiangle of 20–30° was reported for both probes, which is comparable to the value we obtained for our bifunctional labeled kinesin construct (32 ± 5^{o}). However the value we obtained for our monofunctional probe (50 ± 5^{o}) is much larger. These differences could be attributed to differences in the bifunctional probes used, proteins used, or method to estimate the cone angle. A key difference between our measurements and the one of Corrie et al. is the time scale on which order and disorder is probed. In our experimental set up, the time scale of the measurement is 100 ms, whereas, in Corrie et al., the time scale is on the order of the fluorescence lifetime (several nanoseconds). Therefore, it is possible that the extra mobility that we observe for the monofunctional probe takes place on a far longer time scale than the fluorescence lifetime. This notion is in agreement with our observation that the bulk fluorescence anisotropy (which probes disorder on the time scale of the fluorescence lifetime) is similar (0.25) whether the bifunctional or monofunctional probe is used (data not shown).

A drawback of using a bifunctional probe with relatively rigid linkers is that the distance between the target residues in the protein is critical. We found by trial and error that, in our case, a distance of 5 residues (16 Å), in a non-α helical region, leads to optimal and good labeling yields.

There is also a significant difference in the axial angle for the construct labeled with BSR (75°) and the ones with TMR (56^{o} and 58°). This is most likely due to the different position of the thiol-reactive group(s) on the probes (Fig. 1 *A*), resulting in a different orientation of the probe with respect to the protein.

Orientation of KMC2-BSR on microtubules

Apart from the more rigid attachment, an important additional advantage of using a bifunctional probe attached to two predefined locations on the protein is that the orientation of the transition dipole relative to the protein structure is known (when the atomic structure of the protein is available and the structure does not change dramatically for the functionalized mutant) (Corrie et al., 1999). In our case, this allows us to relate the measured axial angle between probe and axoneme to the orientation of the kinesin motor domain bound to the microtubule. An axial angle of 75°, as determined in this study, is within the range expected from models of the kinesin–microtubule complex in the presence of AMP-PNP, derived from cryo-electron microscopy (Fig. 1 *B*). The good agreement between the orientations of kinesin determined by these two different methods supports their validity. It should be pointed out though, that, based on cryo-electron microscopy, three different docking models for the interaction of kinesin motors with microtubules have been proposed. One model is the one shown in Fig. 1 *B*, which has been proposed for the ATP state (mimicked by the presence of AMP-PNP) of three different kinesin-type motors, ncd (Sosa et al., 1997), conventional kinesin (Hoenger et al., 1998), and KIF1A (Kikkawa et al., 2000). The other two orientations have been proposed for conventional kinesin or ncd in the presence of ADP (Kozielski et al., 1998; Hirose et al., 1999). The three alternative models differ mainly in the azimuthal orientation of the motor domain (angular orientation around an axis centered on the motor and parallel to the microtubule long axis). Our fluorescence measurements are sensitive only to the axial angle of the fluorophore with the axoneme (β) but not its azimuthal orientation. Thus, either of the three models would be equally consistent with our data, and we cannot distinguish between them. However, in one of the models (Kozielski et al., 1998) the probes on our labeled constructs would be facing the microtubule, possibly interfering with binding. This model then seems inconsistent with the fact that our labeled constructs bind to microtubules and show normal ATPase activity. It is also possible that the orientation of kinesin relative to the microtubule in the presence of ADP or AMP-PNP is different. A change in the motor domain orientation depending on nucleotide has been reported for KIF1A (Kikkawa et al., 2001) (without major changes in the azimuthal orientation, though). It is also possible that, in the presence of ADP, due to the weak interaction of the motor with the microtubule (Crevel et al., 1996), the orientation of the motor domain is not well defined. In fact, in a previous fluorescence polarization study of conventional kinesin bound to microtubules, we have shown that the motor possesses a high degree of angular mobility in the presence of ADP (Sosa et al., 2001).

Comparison between the monomeric and dimeric kinesin constructs

Both the dimeric and monomeric kinesin constructs labeled with the monofunctional probe (KMC-TMR and KCL-

TMR) showed similar mobility values ($r_{aver} = 0.4$, $\Gamma = 50^o$). Also the calculated axial angle of the probe was very similar in both cases (56^o for KMC-TMR and 58^o for KCL-TMR). This result indicates no difference in mobility and only a small difference in orientation whether individual kinesin molecules are bound to the microtubule (monomers) or whether kinesin dimers are bound. This finding indicates that, in the presence of AMP-PNP, the orientation of the two heads in a kinesin dimer bound to a microtubule is similar to the orientation of a monomeric kinesin head bound to a microtubule.

Cryo-electron microscopy-based three-dimensional reconstructions of dimeric kinesin constructs bound to microtubules in the presence of AMP-PNP usually show the microtubule attached head and either a smaller adjacent density (Arnal et al., 1996; Hirose et al., 1996) or no density at all (Hoenger et al., 1998) corresponding to the partner head. These results have been interpreted in two ways: 1) one head is bound to the microtubule and the partner head is unbound and disordered (Arnal et al., 1996; Hirose et al., 1996), or 2) both heads are bound with the same configuration to contiguous binding sites in the microtubule (Hoenger et al., 1998, 2000). Our results support the second interpretation. If the dimeric kinesin would have one head attached and the second one disordered, we would have expected higher mobility for the dimeric construct when compared to the monomeric one. We instead observed similar mobility for both constructs. Therefore, our results indicate that, in the presence of AMP-PNP, both heads of a kinesin dimer are bound simultaneously to the microtubule. In many cryo-electron microscopy experiments, an excess of kinesin over tubulin binding sites may impede one of the heads of the dimer to bind (Hoenger et al., 2000). This concern is not present in our fluorescence polarization experiments, where we used an excess of at least four fold of tubulin binding sites over kinesin heads (see Methods). Recent measurements of the binding forces of kinesin molecules bound to microtubules also support the conclusion that the two heads of dimeric kinesin bind to the microtubule in the presence of AMP-PNP (Kawaguchi and Ishiwata, 2001). A double-attached state for kinesin is required in models, such as the hand-over-hand (Hackney, 1994), that explains kinesin processivity by the coordinated action of the two motor domains.

APPENDIX

The linear dichroism of many kinesin motors labeled with perfectly fixed fluorescent probes and attached to an axoneme

We start with a dipole in the xy-plane, which makes an angle β with an axoneme along the x axis. First, this dipole is rotated through an angle ϵ around the axoneme long axis (the x axis). Second, the axoneme, including the attached dipole, is rotated around the z axis with an angle ω. The rotated dipole ($\mu(\beta, \epsilon, \omega)$) can be expressed as

$$\vec{\mu}(\beta, \varepsilon, \omega) = \begin{pmatrix} \cos(\omega) & -\sin(\omega) & 0 \\ \sin(\omega) & \cos(\omega) & 0 \\ 0 & 0 & 1 \end{pmatrix} \cdot \begin{pmatrix} 1 & 0 & 0 \\ 0 & \cos(\varepsilon) & -\sin(\varepsilon) \\ 0 & \sin(\varepsilon) & \cos(\varepsilon) \end{pmatrix} \cdot \begin{pmatrix} \cos(\beta) \\ \sin(\beta) \\ 0 \end{pmatrix} = \begin{pmatrix} \cos(\omega)\cos(\beta) - \sin(\omega)\cos(\varepsilon)\sin(\beta) \\ \sin(\omega)\cos(\beta) + \cos(\omega)\cos(\varepsilon)\sin(\beta) \\ \sin(\varepsilon)\sin(\beta) \end{pmatrix} \tag{A1}$$

This is the situation as depicted in Fig. 3 *A*. Our signal (the emission resulting from absorption of light of different polarization) is the square of the inner product of the excitation laser electric field and the transition dipole moment. We are interested in this observable for excitation light polarized along the x- and the y axis in a situation where the axoneme is decorated with many kinesins in all different azimuthal orientations ϵ around the microtubule. Thus, we calculate the square of the projection on the x- ($\langle \mathrm{proj}_x(\beta, \omega)^2 \rangle$) and the y axis ($\langle \mathrm{proj}_y(\beta, \omega)^2 \rangle$) of the dipole moments of many probes, i.e., averaged over all orientations ϵ:

$$\langle \mathrm{proj}_x(\beta, \omega)^2 \rangle = \frac{1}{2\pi} \int_0^{2\pi} \mu_x(\beta, \varepsilon, \omega)]^2 \, d\varepsilon = \cos^2(\omega)\cos^2(\beta) + \tfrac{1}{2}\sin^2(\omega)\sin^2(\beta) \tag{A2}$$

$$\langle \mathrm{proj}_y(\beta, \omega)^2 \rangle = \frac{1}{2\pi} \int_0^{2\pi} \mu_y(\beta, \varepsilon, \omega)]^2 \, d\varepsilon = \sin^2(\omega)\cos^2(\beta) + \tfrac{1}{2}\cos^2(\omega)\sin^2(\beta) \tag{A3}$$

From these equations, the LD can be calculated straightforwardly using Eq. 1:

$$\mathrm{LD}(\beta, \omega) = \frac{\langle \mathrm{proj}_y(\beta, \omega)^2 \rangle - \langle \mathrm{proj}_x(\beta, \omega)^2 \rangle}{\langle \mathrm{proj}_y(\beta, \omega)^2 \rangle + \langle \mathrm{proj}_x(\beta, \omega)^2 \rangle} = \frac{-3\cos(2\omega)}{1 + 4/(3 \cdot \cos^2(\beta) - 1)} \tag{2}$$

The linear dichroism of a randomly oriented dipole that is free to move in a cone

We start with assuming a dipole (with unit length) along the z axis. It should be noted that, in this part of the appendix, "free" dipoles are considered, no axonemes (and cylindrical symmetry) are involved. Now we allow the dipole to assume any orientation within a cone, restrained by a half angle Γ (Lipari and Szabo, 1980). The orientation of the dipole within the cone is described by the polar angle γ' around the y axis (which

can run from 0 to Γ; the prime indicates that this angle is in the frame of the mobility cone) and the azimuthal angle δ′ around the *z* axis (which can run from 0 to 2π). The dipole $\mu(\gamma', \delta')$ can be expressed as

$$\vec{\mu}(\gamma', \delta') = \begin{pmatrix} \cos(\delta') & -\sin(\delta') & 0 \\ \sin(\delta') & \cos(\delta') & 0 \\ 0 & 0 & 1 \end{pmatrix} \cdot \begin{pmatrix} \cos(\gamma') & 0 & \sin(\gamma') \\ 0 & 1 & 0 \\ -\sin(\gamma') & 0 & \cos(\gamma') \end{pmatrix} \cdot \begin{pmatrix} 0 \\ 0 \\ 1 \end{pmatrix} \quad \text{(A4)}$$

$$= \begin{pmatrix} \sin(\gamma') \cdot \cos(\delta') \\ \sin(\gamma') \cdot \sin(\delta') \\ \cos(\gamma') \end{pmatrix}$$

Now we rotate the entire cone away from the *z* axis (around the *y* axis) with polar angle θ (which runs from 0 to π; the absence of a prime indicates that this angle is defined within the lab frame) and around the *z* axis with azimuthal angle φ (which runs from 0 to 2π). This results in a rotated dipole $\mu_{rot}(\gamma', \delta', \phi, \theta)$:

$$\vec{\mu}_{rot}(\gamma', \delta', \phi, \theta) = \begin{pmatrix} \cos(\phi) & -\sin(\phi) & 0 \\ \sin(\phi) & \cos(\phi) & 0 \\ 0 & 0 & 1 \end{pmatrix} \cdot \begin{pmatrix} \cos(\theta) & 0 & \sin(\theta) \\ 0 & 1 & 0 \\ -\sin(\theta) & 0 & \cos(\theta) \end{pmatrix} \cdot \vec{\mu}(\gamma', \delta')$$

$$\vec{\mu}_{rot}(\gamma', \delta', \phi, \theta) \quad \text{(A5)}$$

$$= \begin{pmatrix} \cos(\phi)\sin(\theta)\cos(\gamma') + \cos(\phi)\cos(\theta)\cos(\delta')\sin(\gamma') - \sin(\phi)\sin(\delta')\sin(\gamma') \\ \sin(\phi)\sin(\theta)\cos(\gamma') + \sin(\phi)\cos(\theta)\cos(\delta')\sin(\phi') + \cos(\phi)\sin(\delta')\sin(\gamma') \\ \cos(\phi)\cos(\gamma') + \cos(\theta)\sin(\beta)\sin(\gamma') \end{pmatrix}.$$

Our observables are the average (over all orientations in the cone) of the squares of the projections of the dipole on axes in the *xy*-plane (different excitation polarizations). Assuming an excitation polarization axis (in the *xy*-plane) which makes angle η (in our case 0°, 30°, 45°, 90°, 120°, or 135°) with the *x* axis, the average squared projections ($\langle \text{proj}(\phi, \theta, \Gamma)^2 \rangle$) can be written as

$$\langle \text{proj}_\eta(\phi, \theta, \Gamma)^2 \rangle = \int_0^\Gamma \int_0^{2\pi} \left[\vec{\mu}_{rot}(\gamma', \delta', \phi, \theta) \cdot \begin{pmatrix} \cos(\eta) \\ \sin(\eta) \\ 0 \end{pmatrix} \right]^2 \partial\delta' \sin(\gamma') \partial\gamma' \quad \text{(A6)}$$

$$\langle \text{proj}_\eta(\phi, \theta, \Gamma)^2 \rangle = \pi \cdot \left(\frac{2}{3} - \cos(\Gamma) + \frac{\cos^3(\Gamma)}{3} + \cos(\Gamma)\sin^2(\Gamma)\sin^2(\theta)\cos^2(\eta - \phi) \right)$$

The integration factor, $\sin(\gamma')$ in Eq. A6, equalizes the probabilities for all the orientations in the cone. Using Eqs. A6 and 1, the LD can be expressed for light polarized on any two perpendicular axes in the *xy*-plane as

$$\text{LD}_{\eta - \eta + 90°}(\phi, \theta, \Gamma) = \frac{3 \sin^2(\theta)[2 \cos^2(\phi - \eta) - 1]}{3 \cos^2(\theta) - 1 - 4/[\cos(\Gamma) + \cos^2(\Gamma)]} \quad (4)$$

The linear dichroism of many kinesin motors on an axoneme with fluorescent probes that are free to move within a cone

The squares of the projection of the dipoles on the *x* and *y* axes can be calculated by filling in the possible angles of θ and φ in the many kinesin bound to axoneme case (Eqs. A2 and A3) in the equation of these projections for a general dipole (Eq. A6). We note here that, for the projections on the *x* and *y* axes (in which cases η is 0 or π/2, respectively) the term $\sin^2(\theta)\cos^2(\eta - \phi)$ in Eq. A6 simplifies to $\sin^2(\theta)\cos^2(\phi)$ and $\sin^2(\theta)\sin^2(\phi)$, respectively. These terms are simply the squares of the *x* and *y* projections of the axis of the cone of a given dipole. Here we replace these terms by the average *x* and *y* projections (Eqs. A2 and A3) for the many kinesins bound to axoneme system. The squares of the projections on the *x* and *y* axes, averaged over all orientations around the axoneme can be expressed as

$$\langle \text{proj}_{x/y}(\Gamma, \beta, \omega)^2 \rangle \quad \text{(A7)}$$

$$= \pi \cdot \left(\frac{2}{3} - \cos(\Gamma) + \frac{\cos^3(\Gamma)}{3} + \cos(\Gamma)\sin^2(\Gamma)\langle \text{proj}_{x/y}(\beta, \omega)^2 \rangle \right)$$

In which $\langle \text{proj}_{x/y}(\beta, \omega)^2 \rangle$ is given by Eqs. A2 or A3. From these projections, the LD can be calculated straightforwardly using Eq. 1 and expressed as

$$\text{LD}(\Gamma, \beta, \omega) = \frac{-3 \cos(2\omega)}{1 + 8/[3 \cos^2(\beta) - 1] \cdot [\cos(\Gamma) + \cos^2(\Gamma)]} \quad (3)$$

We thank R. Sakowicz for axoneme preparations, advice and discussions, R. Dickson, R. Vale, and D. Pierce for their advice in the initial phases of this project, L. Gross, H. Deng, and L. Siconolfi-Baez, for mass spectrometry analysis, A. Asenjo for biochemical assays, and S. Brasselet and B. Lounis for helpful discussions and experimental suggestions.

L. S. B. Goldstein is an investigator of the Howard Hughes Medical Institute. This project was supported by National Science Foundation grants DMR-9612252 and MCB-9816947.

REFERENCES

Adachi, K., R. Yasuda, H. Noji, H. Itoh, Y. Harada, M. Yoshida, and K. Kinosita, Jr. 2000. Stepping rotation of F1-ATPase visualized through angle-resolved single-fluorophore imaging. *Proc. Natl. Acad. Sci. U.S.A.* 97:7243–7247.

Arnal, I., F. Metoz, S. DeBonis, and R. H. Wade. 1996. Three-dimensional structure of functional motor proteins on microtubules. *Curr. Biol.* 6:1265–1270.

Cantor, C. R., and P. R. Schimmel. 1980. Biophysical Chemistry. Part II, Techniques for the Study of Biological Structure and Function. W.H. Freeman and Co., New York.

Corrie, J. E. T., B. D. Brandmeier, R. E. Ferguson, D. R. Trentham, I. Kendrick-Jones, S. C. Hopkins, U. A. van der Heide, Y. E. Goldman, C.

Sabido-David, R. E. Dale, S. Criddle, and M. Irving. 1999. Dynamic measurement of myosin light-chain-domain tilt and twist in muscle contraction. *Nature.* 400:425–430.

Crevel, I. M., A. Lockhart, and R. A. Cross. 1996. Weak and strong states of kinesin and ncd. *J. Mol. Biol.* 257:66–76.

Funatsu, T., Y. Harada, M. Tokunaga, K. Saito, and T. Yanagida. 1995. Imaging of single fluorescent molecules and individual ATP turnovers by single myosin molecules in aqueous solution. *Nature.* 374:555–559.

Gibbons, I. R., and E. Fronk. 1979. A latent adenosine triphosphatase form of dynein 1 from sea urchin sperm flagella. *J. Biol. Chem.* 254:187–196.

Goldstein, L. S. B., and A. V. Philp. 1999. The road less traveled: emerging principles of kinesin motor utilization. *Annu. Rev. Cell Dev. Biol.* 15:141–183.

Ha, T., T. A. Laurence, D. S. Chemla, and S. Weiss. 1999. Polarization spectroscopy of single fluorescent molecules. *J. Phys. Chem. B.* 103: 6839–6850.

Hirose, K., A. Lockhart, R. A. Cross, and L. A. Amos. 1996. Three-Dimensional Cryoelectron Microscopy of Dimeric Kinesin and Ncd Motor Domains On Microtubules. *Proc. Natl. Acad. Sci. U.S.A.* 93: 9539–9544.

Hirose, K., J. Lowe, M. Alonso, R. A. Cross, and L. A. Amos. 1999. Congruent docking of dimeric kinesin and ncd into three-dimensional electron cryomicroscopy maps of microtubule-motor ADP complexes. *Mol. Biol. Cell.* 10:2063–2074.

Hoenger, A., S. Sack, M. Thormählen, A. Marx, J. Müller, H. Gross, and E. Mandelkow. 1998. Image reconstructions of microtubules decorated with monomeric and dimeric kinesins: comparison with x-ray structure and implications for motility. *J. Cell Biol.* 141:419–430.

Hoenger, A., M. Thormahlen, R. Diaz-Avalos, M. Doerhoefer, K. N. Goldie, J. Muller, and E. Mandelkow. 2000. A new look at the microtubule binding patterns of dimeric kinesins. *J. Mol. Biol.* 297: 1087–1103.

Kawaguchi, K., and S. Ishiwata. 2001. Nucleotide-dependent single- to double-headed binding of kinesin. *Science.* 291:667–669.

Kikkawa, M., Y. Okada, and N. Hirokawa. 2000. 15 angstrom resolution model of the monomeric kinesin motor, KIF1A. *Cell.* 100:241–252.

Kikkawa, M., E. P. Sablin, Y. Okada, H. Yajima, R. J. Fletterick, and N. Hirokawa. 2001. Switch-based mechanism of kinesin motors. *Nature.* 411:439–445.

Kozielski, F., I. Arnal, and R. H. Wade. 1998. A model of the microtubule–kinesin complex based on electron cryomicroscopy and x-ray crystallography. *Curr. Biol.* 8:191–198.

Kull, F. J., E. P. Sablin, R. Lau, R. J. Fletterick, and R. D. Vale. 1996. Crystal structure of the kinesin motor domain reveals a structural similarity to myosin. *Nature.* 380:550–555.

Lipari, L., and A. Szabo. 1980. Effect of librational motion on fluorescence depolarization and nuclear magnetic resonance relaxation in macromolecules and membranes. *Biophys. J.* 30:489–506.

Lu, H. P., L. Xun, and X. S. Xie. 1998. Single-molecule enzymatic dynamics. *Nature.* 282:1877–1882.

Moerner, W. E., and M. Orrit. 1999. Illuminating single molecules in condensed matter. *Science.* 283:1670–1674,1675–1676.

Penzkofer, A., and J. Wiedmann. 1980. Orientation of transition dipole moments of rhodamine 6G determined by excited state absorption. *Opt. Commun.* 35:81–86.

Rice, S., A. W. Lin, D. Safer, C. L. Hart, N. Naber, B. O. Carragher, S. M. Cain, E. Pechatnikova, E. M. Wilson-Kubalek, M. Whittaker, E. Pate, R. Cooke, E. W. Taylor, R. A. Milligan, and R. D. Vale. 1999. A structural change in the kinesin motor protein that drives motility. *Nature.* 402: 778–784.

Sase, I., H. Miyata, S. Ishiwata, and K. Kinosita, Jr. 1997. Axial rotation of sliding actin filaments revealed by single-fluorophore imaging. *Proc. Natl. Acad. Sci. U.S.A.* 94:5646–5650.

Sosa, H., D. P. Dias, A. Hoenger, M. Whittaker, E. WilsonKubalek, E. Sablin, R. J. Fletterick, R. D. Vale, and R. A. Milligan. 1997. A model for the microtubule-Ncd motor protein complex obtained by cryo-electron microscopy and image analysis. *Cell.* 90:217–224.

Sosa, H., E. J. G. Peterman, W. E. Moerner, and L. S. Goldstein. 2001. ADP-induced rocking of the kinesin motor domain revealed by single-molecule fluorescence polarization microscopy. *Nat. Struct. Biol.* 8:540–544.

Vale, R. D., and R. A. Milligan. 2000. The way things move: looking under the hood of molecular motor proteins. *Science.* 288:88–95.

van Amerongen, H., and W. S. Struve. 1995. Polarized optical spectroscopy of chromoproteins. *Methods Enzymol.* 246:259–283.

Warshaw, D. M., E. Hayes, D. Gaffney, A. M. Lauzon, J. Wu, G. Kennedy, K. Trybus, S. Lowey, and C. Berger. 1998. Myosin conformational states determined by single fluorophore polarization. *Proc. Natl. Acad. Sci. U.S.A.* 95:8034–8039.

Weiss, S. 1999. Fluorescence spectroscopy of single biomolecules. *Science.* 283:1676–1683.